

# Probing Water Diffusion Inside Crystals of AlPO-5 by PFG NMR and IRM for Heat Storage Applications

Muslim Dvoyashkin\*, Christian Chmelik, Thomas Nonnen, Ralph Hermann,  
Margarita Russina, and Roger Gläser\*

DOI: 10.1002/cite.202300072

 This is an open access article under the terms of the Creative Commons Attribution-NonCommercial-NoDerivs License, which permits use and distribution in any medium, provided the original work is properly cited, the use is non-commercial and no modifications or adaptations are made.

**Dedicated to Prof. Dr. rer. nat. Jörg Kärger on the occasion of his 80th birthday**

Diffusion of water in the aluminophosphates AlPO-5 is studied using a combination of pulsed field gradient NMR and IR microimaging. The concentration profiles measured by the latter allowed to visualize the process of water sorption and propagation into the crystals of AlPO-5. The self-diffusion coefficients obtained by NMR were one order of magnitude higher values compared to corrected ones from the IR microimaging study. The concentration profiles allowed to visualize the process of water sorption and propagation into the crystals of AlPO-5. The obtained results are compared with experimental and simulation data for the water/AlPO-5 system for the literature and discussed in the context of its potential use for heat storage applications.

**Keywords:** AlPO-5, Diffusion, IR microimaging, Pulsed field gradient NMR, Water

Received: April 19, 2023; revised: July 20, 2023; accepted: July 26, 2023

## 1 Introduction

The supply of heat from regenerative sources is among challenges that are yet to be solved as part of the energy transition towards its higher sustainability [1]. There is also a need for research and development in the storage of thermal energy, which should be stored seasonally with as little loss as possible. One possible way to accomplish this is to utilize thermochemical storage systems, in which the heat is stored through reversible physical-chemical processes of adsorption and desorption [2, 3]. This topic focusing on the adsorptive heat transformations is of growing interest for heat storage, heat pumps and thermally driven cooling [4–6]. By using solar or waste heat as energy source, such systems can make a significant contribution to minimizing primary energy consumption and greenhouse gas emissions in buildings and industrial processes. In adsorptive heat transformation, a working medium, preferably water, is cycled in a closed system between a liquid phase and an adsorbed phase. The adsorbents are generally solid micro- and mesoporous materials. The heat of adsorption, which is released during the adsorption of the working fluid in the pore system, represents the waste heat in a cooling application or the usable heat in a heat pump. In both cases, the regeneration of the system requires a desorption of the working fluid at higher temperature (> 338 K), for which,

e.g., solar energy or waste heat from industrial processes can be used.

The systems using this technology were earlier built by German companies and are currently available on the market, mainly for (solar or waste heat) cooling (commercialized, e.g., by Fahrenheit) [7] or gas heat pumps (commercialized, e.g., by Vaillant). In these systems, zeolites or silica gel are used as sorbents. The adsorption and desorption of

---

<sup>1,2</sup>Dr. habil. Muslim Dvoyashkin

<sup>1</sup><https://orcid.org/0000-0003-4411-1952> (muslim.dvoyashkin@uni-leipzig.de), <sup>3</sup>Dr. Christian Chmelik,

<sup>4</sup>Dr. Thomas Nonnen, <sup>4</sup>Dr. Ralph Hermann,

<sup>5</sup>Dr. Margarita Russina, <sup>2</sup>Prof. Dr. Roger Gläser

<sup>2</sup><https://orcid.org/0000-0002-8134-4280> (roger.glaeser@uni-leipzig.de)

<sup>1</sup>Leipzig University, Institute of Analytical Chemistry, Linnestraße 3, 04103 Leipzig, Germany

<sup>2</sup>Leipzig University, Institute of Chemical Technology, Linnestraße 3, 04103 Leipzig, Germany.

<sup>3</sup>Leipzig University, Faculty of Physics and Earth Sciences, Linnestraße 5, 04103 Leipzig, Germany.

<sup>4</sup>Fahrenheit GmbH, Zscherbener Landstraße 17, 06126 Halle (Saale), Germany.

<sup>5</sup>Helmholtz-Zentrum Berlin für Materialien und Energie, 14109 Berlin, Germany.

the working medium in the system requires that the molecules enter the pore system of the respective adsorbent. This mass transport is a diffusion process. At the same time, heat is released (or required) and must be supplied or removed from the porous sorbent. Thus, the diffusive mass transport and the heat transfer are coupled by the sorption processes. Methods for understanding fundamental questions of adsorption and diffusion of water in SAPO-34 (zeotype sorbent) crystallized directly on a porous fiber structure were developed [8]. This contribution by Stallmach et al. represents a significant step towards understanding of water diffusion in heat-storage materials. Benefiting from the combined application of pulsed field gradient (PFG) NMR and infrared microimaging (IRM), authors demonstrated that corrected diffusivities determined by IRM during adsorption and desorption and the self-diffusion coefficients derived from NMR diffusion studies are both independent of water loading and about two orders of magnitude smaller than the diffusivity of liquid water at the same temperature. Other promising sorbents have also been investigated in terms of water sorption equilibria and dynamics [9–11].

Previously, it was found that water diffusion in the compact sorbent crystallite layer can be the dominant process in such a sorption heat exchanger [12]. However, it was recognized that the transport parameters differ by orders of magnitude depending on the material and its configuration in the sorption heat exchanger. The operation and the possible improvement in performance of such sorption heat exchangers require both profound knowledge of the diffusion processes on the size scale of the microporous adsorbent crystallites and the micro- and mesoporous adsorbent layer as well as well-validated macroscopic models, by which the performance on the adsorption heat exchanger level can be predicted.

The efficiency of the adsorption process is primarily determined by the density, the pore geometry and the accessibility of the framework of the sorbent used, the interaction energy with the sorption sites on the pore walls and the thermophysical properties such as heat capacity and thermal conductivity [13]. It is further influenced by the support structure on which the active sorbent is applied and by the available temperature boundary conditions. Common technologies with regard to the adsorption heat exchanger are either loose packing or binder-based coatings in finned or finned tube heat exchangers, state of the art is direct growth of aluminophosphate layers by partial support transformation (PST) on dedicated heat exchangers.

In addition to aluminophosphates and zeolites [6, 14–17], which are highly interesting from an industrial point of view for heat storage applications, metal-organic frameworks (MOFs) are attracting more and more attention because of their high specific pore volume and chemical diversity [11, 12]. However, different MOFs show either a continuous or a sudden structural change of the crystal framework caused by water adsorption. Because of these

so-called “breathing” or “gate-opening” effects, the adsorption and diffusion mechanisms in such materials are of particular interest, but highly demanding in terms of experimental and theoretical description. From the large variety of proposed and synthesized MOF structures, the water-stable iron or aluminum trimesate MIL-100(Fe,Al), CAU-10-H, MIL-101(Cr) were identified as a particularly promising representative for adsorptive heat conversion [18, 19].

For a number of related microporous adsorbent materials, such as zeolites, there have been developed experimental [13–15] and theoretical [16] methods to characterize the diffusion of guest molecules. Kärger et al. succeeded to utilize the PFG NMR to measure the self-diffusion of water and Li-ions in meso- and macroporous glasses and in microporous LSX zeolites [20, 21]. Molecular dynamics (MD) simulations and experimental studies performed using PFG NMR and IRM were combined to elucidate the diffusion of carbon dioxide and methane as a function of loading in ZIF-8 [22, 23].

In this contribution, the diffusion of water in crystals of microporous aluminophosphate AlPO-5 was probed by PFG NMR and IR microimaging. Measurements at different temperatures allowed determination of activation energy for diffusion. Results obtained by these two techniques are compared and discussed in the context of heat storage applications.

## 2 Experimental

### 2.1 Preparation and Characterization of AlPO-5 Materials

Since traces of iron are known to reduce relaxation times in PFG NMR measurements, special care was taken in order to keep traces of iron in the sample as low as possible by using newly purchased glass equipment and Teflon stirrers, non-metal spatulas, and thoroughly cleaned Teflon liners in the autoclave. AlPO-5 was crystallized on aluminum plates (Alloy EN AW-1050A) using the PST method. The synthesis procedure was developed by Fahrenheit GmbH [49]. 32.0 g of phosphoric acid (85 %, Brenntag) were diluted in 327.0 g of deionized water under stirring. Then 31.9 g of triethylamine (TEA, 99 %, Büfa) were slowly added under vigorous stirring. 36.33 g of deionized water were added, and the mixture stirred for at least 15 min. The resulting molar ratio was 1  $P_2O_5$  : 2.25 TEA : 150  $H_2O$ . Ten aluminum plates (each 60×60×1 mm) were cleaned with acetone/*i*-propanol (50:50) and dried at room temperature. The plates were placed vertically into a Teflon-lined 1-L-autoclave. The synthesis mixture was added and the hydrothermal synthesis was performed at 463 K for 20 h. After cooling down of the autoclave, the plates were cleaned with deionized water. The excess powder was filtered and washed with deionized water. After cooling down of the

autoclave, the plates were cleaned with deionized water. The excess powder was filtered and washed with deionized water. An additional batch of AlPO-5 crystals were prepared according to procedure described in [24] for NMR experiments to check reproducibility of diffusion data and having possibility to compare it with already reported diffusivities obtained by quasielastic neutron scattering elsewhere (QENS) [25] on the same kind of aluminophosphates.

AlPO-5 powder was synthesized following the synthesis procedure of [26]. Pseudoboehmite (Apyral) was used as the aluminum source. 44.37 g Apyral were added to 269.35 g of deionized water and stirred for 1 h. Then 85.0 g phosphoric acid were added to the mixture and stirred for another 30 min. 56.5 g TEA and 29.93 g deionized water were added while cooling the beaker in a water bath. The resulting molar ratio was 1 Al<sub>2</sub>O<sub>3</sub> : 1 P<sub>2</sub>O<sub>5</sub> : 1.5 TEA : 50 H<sub>2</sub>O. After stirring for another 2 h, the synthesis mixture was transferred to a Teflon-lined 1-L-autoclave and heated to 453 K for 36 h. The resulting powder was filtered, washed with deionized water and dried at room temperature. Plates were calcined (thermal removal of the template) at 823 K whereas powder was calcined at 873 K. AlPO-5 mass on the supports was estimated by the mass loss during calcination. Crystal phase was confirmed by X-ray diffraction.

Prior to diffusion measurements, AlPO-5 crystals were analyzed by energy dispersive X-ray spectroscopy on the scanning electron microscopy (SEM-EDX). Fig. 1 shows SEM images of the successfully synthesized crystals, which exhibit the characteristic AlPO-5 rod-shaped morphology. No iron could be seen by EDX analysis within the detection limits corresponding to ~0.01 wt % (Fig. 2).

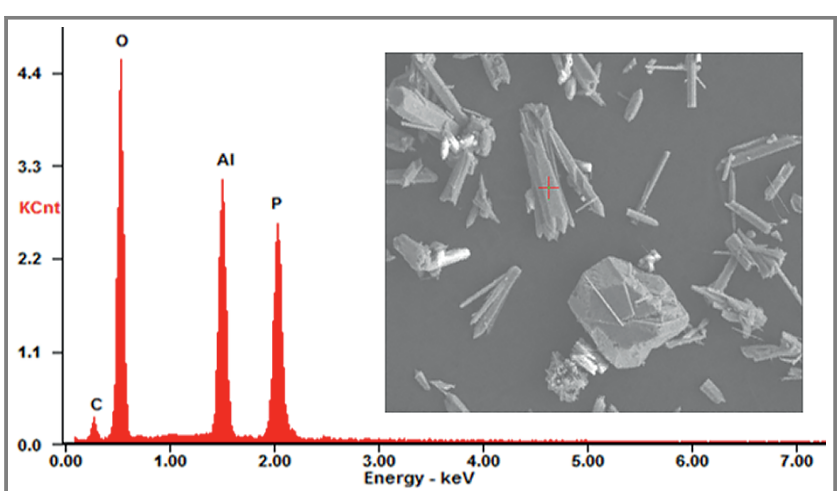


**Figure 2.** SEM-EDX spectrum of AlPO-5 crystals presented in Fig. 1. The inset shows a selected area used for analysis.

## 2.2 Sample Preparation for Diffusion Measurements and Conduction of Diffusion Experiments

The PFG NMR studies were done using a home-built spectrometer operating at 100 MHz for protons and equipped with a pulsed magnetic field gradient unit. For diffusion experiments, the stimulated spin-echo pulse sequence was employed. With this technique, the process of molecular propagation in the direction of the applied magnetic field gradient is monitored during the observation time  $t = (\Delta - \delta/3)$  ms, where  $\Delta = 10$  ms is a separation between two gradient pulses. Other experimentally relevant parameters were separation between first two 90° radio-frequency pulses  $\tau = 1.2$  ms and the duration of the gradient pulses  $\delta = 0.8$  ms. The materials under study, which were placed in NMR glass tubes, were first dried for 6 h at 473 K then kept in contact with the vapor of deionized water (Sigma-Aldrich, ultrapure) overnight at 298 K at a pressure of ~3 kPa corresponding to  $P/P_s = 0.7$  for water. In this way, loading of the pores by gas adsorption was ensured and the amount of adsorbed water corresponded to a relative pore filling of ~1. Preparation of samples at lower loadings was prohibited by too low vapor pressure to achieve reproduc-

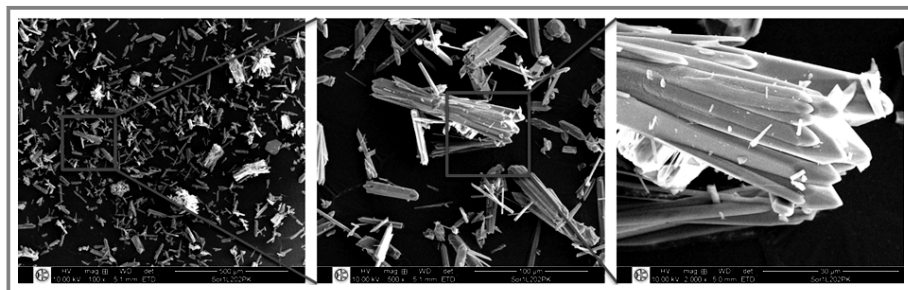


**Figure 1.** SEM images of AlPO-5 crystals at different magnifications. Single crystals with an average size of 5 × 100 µm are visible.

ible water loadings inside NMR tube. Thereafter, the probes were sealed.

Analysis of NMR attenuation curves is done using a two-exponential function [27]:  $\Psi = p_{\text{intra}} \cdot \exp(-\gamma^2 g^2 \delta^2 t D_{\text{intra}}) + (1 - p_{\text{intra}}) \cdot \exp(-\gamma^2 g^2 \delta^2 t D_{\text{inter}})$ , where  $\Psi$  is a measured NMR signal normalized to its maximum value observed in the absence of applied gradients  $g$ ,  $\gamma$  is a gyromagnetic ratio of  $^1\text{H}$  nuclei,  $p_{\text{intra}}$  is a pre-exponential weighting factor,  $D_{\text{intra}}$  and  $D_{\text{inter}}$  represent self-diffusion coefficients of slower and faster diffusing water molecules. The fitting procedure was performed varying parameters  $p_{\text{intra}}$ ,  $D_{\text{intra}}$  and  $D_{\text{inter}}$  until the fit is converged.

To characterize the transport properties of water in the AlPO-5 material a series of IRM and IR micro-imaging measurements was performed. IRM is based on following the intensity of characteristic IR bands of the guest molecules. According to Beer-Lambert law, the absorbance is proportional to the concentration of the absorbing material, e.g. water molecules. In this work a Bruker Hyperion 3000 IR microscope attached to a FT-IR spectrometer (Bruker Vertex 80v) was used [28]. The AlPO-5 material was studied as individual crystals, in small agglomerates of individual crystals and as layered material (Fig. 3, top). For the measurement, typically a few dozens of crystals or a small piece of supported layer was introduced into the IR vacuum cell, attached to a vacuum system and outgassed under vacuum ( $< 10^{-3}$  Pa) at 723 K for at least 18 h (heating

rate  $1 \text{ K min}^{-1}$ ). After cooling of the sample the vacuum cell was mounted on the motorized stage of microscope by keeping the crystals under vacuum. The adsorption or desorption experiments were started by step changes in the gas phase surrounding the crystals (water molecules without any carrier gas). The time evolution of the characteristic IR bands was recorded as integral signal using the single-element (SE) detector. In this work, the band area was calculated in the range of  $3200$ – $3550 \text{ cm}^{-1}$  (Fig. 3, bottom left and middle). Implying the Beer-Lambert law, this area corresponds to the time evolution of the concentration of the absorbed water molecules and by plotting the normalized area over time integral uptake curves are obtained (Fig. 3, bottom right). The uptake curves were fitted by the solution of Fick's 2nd law for diffusion-limited uptake in a parallel sided slab (Fig. 3, bottom right) to obtain the transport (Fickian) diffusivity  $D_T$  [29]:

$$c_{\text{norm}}(t) \approx A_{\text{norm}}(t) = \frac{A(t) - A_0}{A_\infty - A_0} = 1 - \frac{8}{\pi^2} \sum_{n=0}^{\infty} \frac{1}{(2n+1)^2} \exp\left(-\frac{(2n+1)^2 D_T \pi^2 t}{l^2}\right) \quad (1)$$

with  $l$  as length of the crystal (channel length). The first 100 terms were included in the fit.

In addition, time resolved measurements were also performed using the Focal Plane Array (FPA) detector

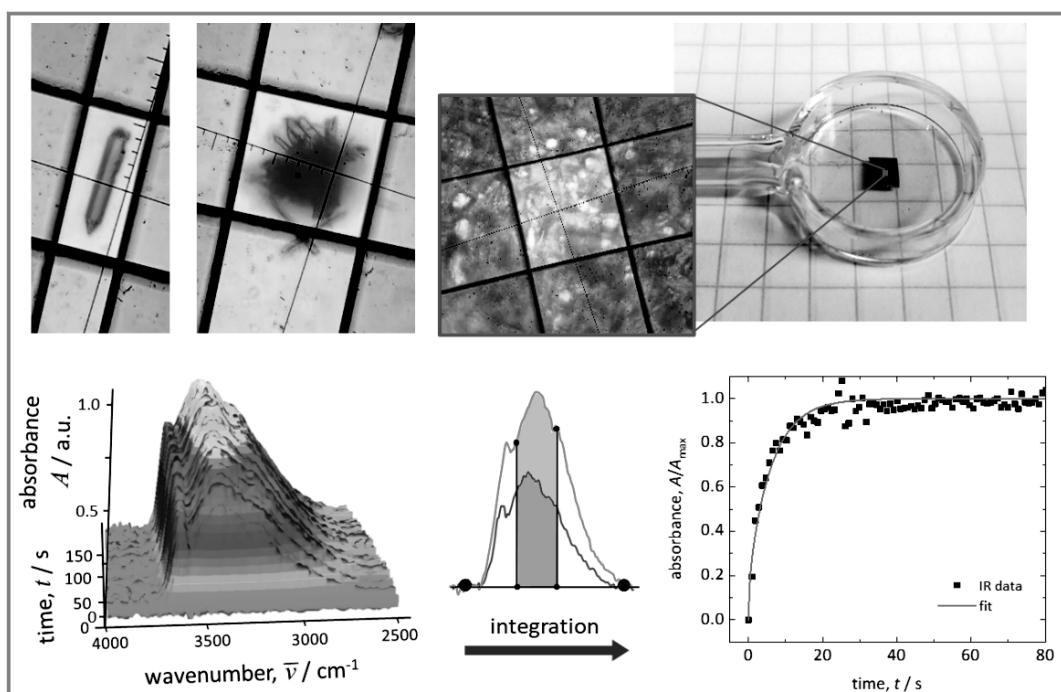


**Figure 3.** Microscopic images of the different AlPO-5 samples used in IRM studies of water transport (from top to right): individual crystals (sample 1; length ca.  $80 \mu\text{m}$ ), agglomerates of crystals (sample 2; average length ca.  $30 \mu\text{m}$ ) and intergrown layers (layer sample; layer thickness ca.  $40 \mu\text{m}$ ). All samples were introduced into an IR quartz glass vacuum cell for the measurements (visual image, right end). From the time-evolution of characteristic IR bands integral uptake curves are obtained and fitted by a solution of Fick's 2nd law for diffusion in one-dimensional channels (bottom left to right).

(effective pixel size  $2.7 \times 2.7 \mu\text{m}^2$ ). Each detector element records an IR spectrum, from which by integration images of the local distribution of the guest molecules can be calculated (see Fig. 7).

### 3 Results and Discussion

#### 3.1 Water Diffusion in AlPO-5

Fig. 4 demonstrates diffusion attenuation curves measured for water in AlPO-5 at full loading at 298 K and 323 K using PFG NMR spectroscopy. It is worth noting that multiply previous attempts with AlPO-5 samples synthesized according to standard synthesis procedure described in, e.g., [30], failed due to too short NMR relaxation times of water protons in the sub millisecond region, presumably due to residual iron content in the aluminum source.

In the investigated field gradient range, it was observed that the diffusion attenuation curves follow a non-exponential decay fitted with a suitable bi-exponential function. In this case a model was applied that takes into two account ensembles of water diffusing inside and outside crystals, with respective diffusivities  $D_{\text{intra}}$  and  $D_{\text{inter}}$  accordingly. Unfortunately, moderate signal-to-noise levels did not allow to analyze the diffusion anisotropy by application of powder

averaged spin-echo attenuation expression for unidimensional systems, as described in, e.g., [31] (Eq. 1) or [32] (Eq. 3), since anisotropic one-dimensional diffusion inside the channels of AlPO-5 can be expected. Instead, here one obtains the averaged value for the self-diffusion coefficient of water inside crystals resulting in  $(3 \pm 1) = 10^{-11} \text{ m}^2\text{s}^{-1}$  at 298 K and  $(7 \pm 2) = 10^{-11} \text{ m}^2\text{s}^{-1}$  at 323 K. This corresponds to a slow down by almost two orders of magnitude compared to the free liquid [33]. Such a significant decrease of water mobility with respect to bulk free water is caused by the pore confinement being of comparable size with adsorbed water molecules. The value at 298 K appeared to be very close to the one obtained by QENS in a single experimental report on direct measurement of water diffusivities in AlPO-5 reported previously [25]. Under similar conditions (295 K and full hydration), authors reported  $(3.45 \pm 0.2) = 10^{-11} \text{ m}^2\text{s}^{-1}$ , being also consistent with translational diffusion coefficient of  $(2.4 \pm 0.2) = 10^{-11} \text{ m}^2\text{s}^{-1}$  estimated previously using molecular dynamic simulations for zeolite of a similar structure [34].

Interestingly, in a rich set of data reported over a period of few decades by groups of J. Kärger and H. Jobic on various adsorbate-zeolite systems, the diffusivities seen by neutron scattering were often higher, which was attributed to orders of magnitude smaller length scale typically probed by this technique compared to PFG NMR when the same guest-host system is used [35–41]. Thus, larger molecular displacements seen by latter technique contain impact of structural imperfections of the framework or even crystal defects on molecular transport. In this contribution, from proximity of diffusivities obtained here and in [25] one may conclude that on the scale of  $\sim 1 \mu\text{m}$  corresponding to a root mean square displacement of water at 298 K, no significant impact of defects on water diffusion is observed.

The self-diffusion coefficients presented as a function of the inverse temperature (Fig. 4b) resulted in an estimated apparent activation energy for diffusion of  $(27 \pm 2) \text{ kJ mol}^{-1}$ . This terminology is needed to emphasize that it is determined using only two values of measured self-diffusion coefficients  $D_{\text{intra}}$ . This value is about 15 % smaller than the activation energy estimated by IRM for small loadings in a Fahrenheit synthesized film sample (see Fig. 5, left). At the same time, the self-diffusion coefficients measured by PFG NMR are about one order of magnitude higher than the values estimated as corrected diffusion coefficients for high loadings using IRM (Fig. 5, right). The corrected diffusivities  $D_0$  were calculated from transport (Fickian) diffusivity  $D_T$  and the thermodynamic factor  $\Gamma$  obtained from the equilibrium sorption isotherms by using the equation  $D_0 = D_T/\Gamma = D_T d(\ln c)/d(\ln p)$  [29]. This equation, which is often referred to as “Darken equation”, results from comparing the Fickian approach to diffusion with a more fundamental approach based on the work of Maxwell, Stefan and Einstein, in which the chemical potential is considered as driving force for molecular fluxes. Here,  $\Gamma$  is defined via the fugacity  $f$  by  $\Gamma = \partial(\ln f)/\partial(\ln c)$  and the corrected diffusivity

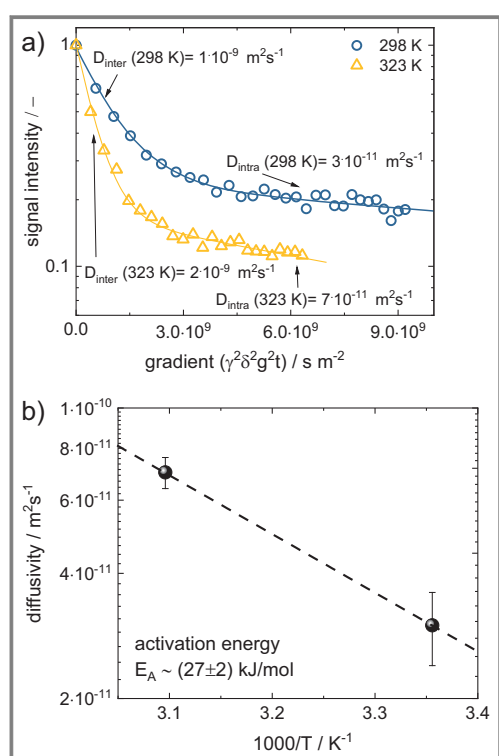


**Figure 4.** a) Diffusion attenuation curves measured for water in AlPO-5 at 298 K and 323 K. Solid lines represent a bi-exponential fit of the signal with respective diffusivities inside ( $D_{\text{intra}}$ ) and outside pores ( $D_{\text{inter}}$ ). b) Values of  $D_{\text{intra}}$  plotted as a function of reciprocal temperature with the dashed line connecting them.

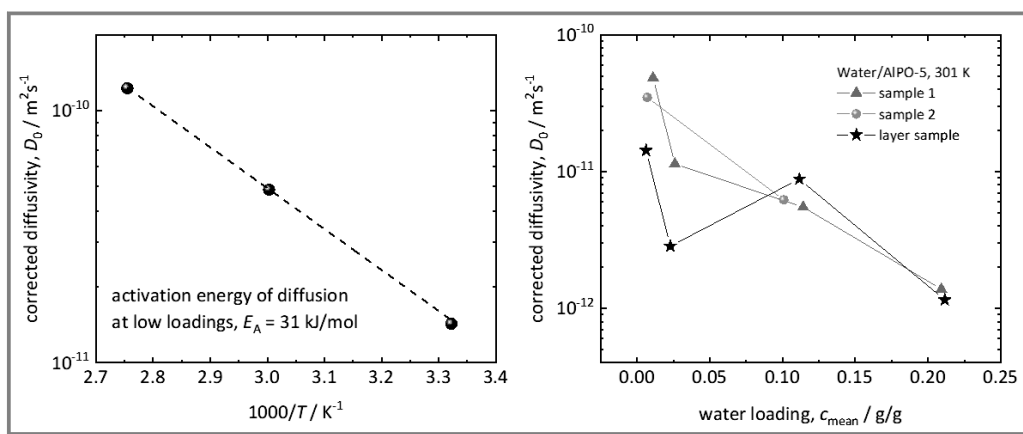


**Figure 5.** Temperature dependence of the diffusion coefficients for water in AlPO-5 estimated at low loadings ( $< 0.01 \text{ g g}^{-1}$ ) by IRM. Assuming Arrhenius behavior, the result is a comparatively high activation energy  $E_A$  of approx.  $31 \text{ kJ mol}^{-1}$  (left). The corrected diffusion coefficients  $D_0$  estimated from IRM and gravimetric isotherm data exhibit a pronounced and essentially linear decrease with increasing loading (right).

is identical to the Maxwell-Stefan diffusivity for single components [29, 42]. By neglecting deviations from the ideal gas law (which are in fact insignificant at the given temperatures and pressures), the fugacity may be identified with the partial pressure and thus  $\Gamma$  can be calculated directly from the equilibrium sorption isotherm [29]. Due to correlation effects, it can be assumed that the corresponding self-diffusion coefficients are even slightly smaller than the corrected diffusion coefficients.

While the activation energies determined by PFG NMR and IRM are in a good agreement, the differences in the diffusion coefficients may indicate the existence of defects on the scale of few tens of micrometers, i.e., not achievable in the PFG NMR experiment due to short relaxation times preventing longer observation times. Bottlenecks in the channels (e.g. "stacking faults" as in MOR zeolites) would be conceivable, either as a specific feature of the crystals, or with a distance significantly above the typically achieved

molecular shifts in PFG NMR measurements. The existence of bottlenecks might also contribute to slightly higher activation energy for diffusion found in the IRM measurements. A similarly high activation energy was estimated previously for water in SAPO-34 with a limiting window diameter of approx.  $0.4 \text{ nm}$  [8].

The IR absorbance data were calibrated by comparing equilibrium adsorption isotherms measured by gravimetric uptake and IRM (Fig. 6, left). While good agreement at low and intermediate loadings is observed, the IR signal notably underestimates the water loading at higher pressures due to saturation effects of the IR band and intermolecular interactions causing deviations from the Beer-Lambert law. Interestingly, a hysteresis loop occurs when following the desorption branch of the isotherm. Similar feature was observed before in this system in other experimental studies [25]. Complementary studies using density functional theory calculations combined by Rietveld refinement of

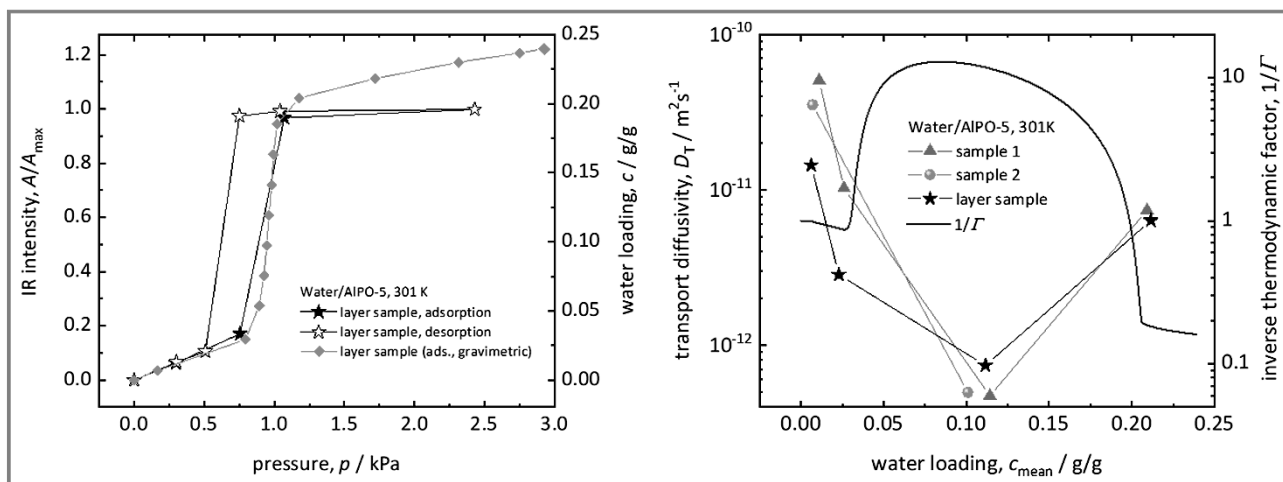


**Figure 6.** Equilibrium sorption isotherms of water in AlPO-5 at 301 K, measured by gravimetric uptake and IRM (left). Loading dependence of transport diffusivity  $D_T$  calculated from the IRM uptake data by implying diffusive uptake in 1d channels (right). The S-shaped isotherm causes a broad maximum larger than unity of the inverse thermodynamic factor  $1/\Gamma = d(\ln c)/d(\ln p)$ .

measured XRD patterns and molecular simulations revealed phase changes in the AlPO-5 structure which may explain the observed sorption hysteresis [43]. It was concluded that upon water uptake the aluminum coordination changes (from 4-coordinated tetrahedra to 6-coordinated octahedra and 5-coordinated bipyramids). The involved structural changes require some energy to overcome the barrier to the other phase. On adsorption-desorption cycles the corresponding pressures (chemical potentials) are difference and, hence, a hysteresis loop is observed. The authors also reported that the structural change is associated with a decrease in the self-diffusivity by about two orders of magnitude.

The uptake rates measured by IRM also slow down by about two orders of magnitude as the steep part of the isotherm is approached (Fig. 6, right). Qualitatively similar trends have been observed previously in systems, where intermolecular interactions of the adsorbed molecules were exceeding their interactions with the host lattice [44]. Indeed, the estimated corrected diffusivities  $D_0$  apparently follow a linear decrease with loading (Fig. 6, right), if the values at water loadings around  $0.025 \text{ g g}^{-1}$  are ignored. A linear decrease of the corrected diffusivity is often observed in pore structures with 1d channels [42]. Hence one may argue that the slowdown is mainly a consequence of adsorption thermodynamics which is accounted for by the thermodynamic factor.

However, we believe that the local drop of  $D_0$  in the loading region of  $0.025 \text{ g g}^{-1}$  is not just an artifact but the consequence of the onset of a water loading dependent structural transformation (phase transitions) of the AlPO-5 structure [43]. The equilibrium loading reached in these experiments was close to, but not yet in the steep part of the isotherm (see e.g. full star symbol at  $0.76 \text{ kPa}$  in Fig. 6 left), hence the corresponding thermodynamic factor is close to 1 (see Fig. 6 right). Upon phase transition, the equilibration of water uptake is then influenced by water transport and by rearrangements of the water molecules and of the host lattice required to approach the energetically most favorable configurations, i.e., by the progression of the phase change. This effect is not taken into account by the model used to calculate the transport diffusivities and, hence, appears as local minima in the plots of  $D_0$ .

This interpretation is supported by the finding that desorption rates were remarkably slowed down compared to adsorption steps at the same loading. While diffusion theory prescribes ad- and desorption curves to be mirror images (for differential loading steps), the absence of this feature indicates that other processes than diffusion are involved – and that the reported values for  $D_T$  and  $D_0$  require a careful interpretation and are better understood as ‘apparent’ diffusivities.

Another peculiarity of the water transport inside AlPO-5 crystals could be observed in IR imaging measurements. The individual crystals apparently consist of two optically indistinguishable halves with different properties in terms

of guest adsorption and diffusion. Although it is known from the literature that AFI type zeolite crystals often consist of several segments [45–48], significant differences in the adsorption and diffusion properties with an asymmetrical distribution within individual crystals are unknown to date.

Fig. 7 shows a series of images recorded at different times during water uptake (top part) and cuts of the transient water loading along the  $c$ -axis ( $z$ -direction) of the crystal (bottom part). The images show the color-coded signal intensity obtained by integrating the IR spectra (see Fig. 3 bottom left and middle) of each detector element. This intensity is assumed to be proportional to the local water loading; blue corresponds to zero loading, purple to high loadings. From these images one-dimensional profiles were obtained by plotting the signal in the center along the (longitudinal)  $z$ -axis of the crystal. By dividing the profiles with the equilibrium profile at  $t = 886 \text{ s}$  normalized profiles were obtained. This representation directly compares the relative changes in the local concentration. It is seen that the left part of the crystal (for  $z$  from  $0$ – $40 \mu\text{m}$ ) is filled in about 1 min (60 s), while the right half of the crystal (for  $z$  from  $40$ – $80 \mu\text{m}$ ) equilibrates in only 5 min (300 s). In both crystal parts the transient water loading profiles exhibit a distinct curvature, which is typically observed in diffusion-limited uptake processes – just with a significantly slower water transport in the right half. These differences in the crystal parts might be attributed to an interplay of variations in the local composition, phase changes and/or different concentration of defects (stacking faults), whose existence the differences between PFG NMR and IRM diffusion data point to. Due to the pronounced diffusion fronts (curved profiles) it can be concluded that such defects are randomly distributed in the channels and are averaged out by the large number of channels on the scale of the spatial resolution of IRM (about  $3 \mu\text{m}$ ).

Both crystal parts show similar differences in the desorption rates for desorption steps from high towards low loading. Interestingly, for adsorption steps in the low loading range no differences in the water mobility could be evidenced in both crystal parts, however the equilibrium loading in the left half of the crystal was about 5 times higher than in the right part. Obviously, the differences in the water mobility are not just caused by steric hindrances and also involve an interplay with the structural changes of the AlPO-5 lattice.

To estimate the (apparent) diffusion coefficients in both crystal areas, uptake curves for both halves of the crystal were plotted separately and fitted using the analytical solution of Fick’s 2nd law for one-dimensional diffusion, taking into account the diffusion currents (i.e., the effective channel length). In this way, diffusion coefficients were determined for the faster half, which were approximately 10–25 times greater than for the slower half (Fig. 8). The averaged diffusivities are in good agreement with those calculated in previous section from integral uptake.

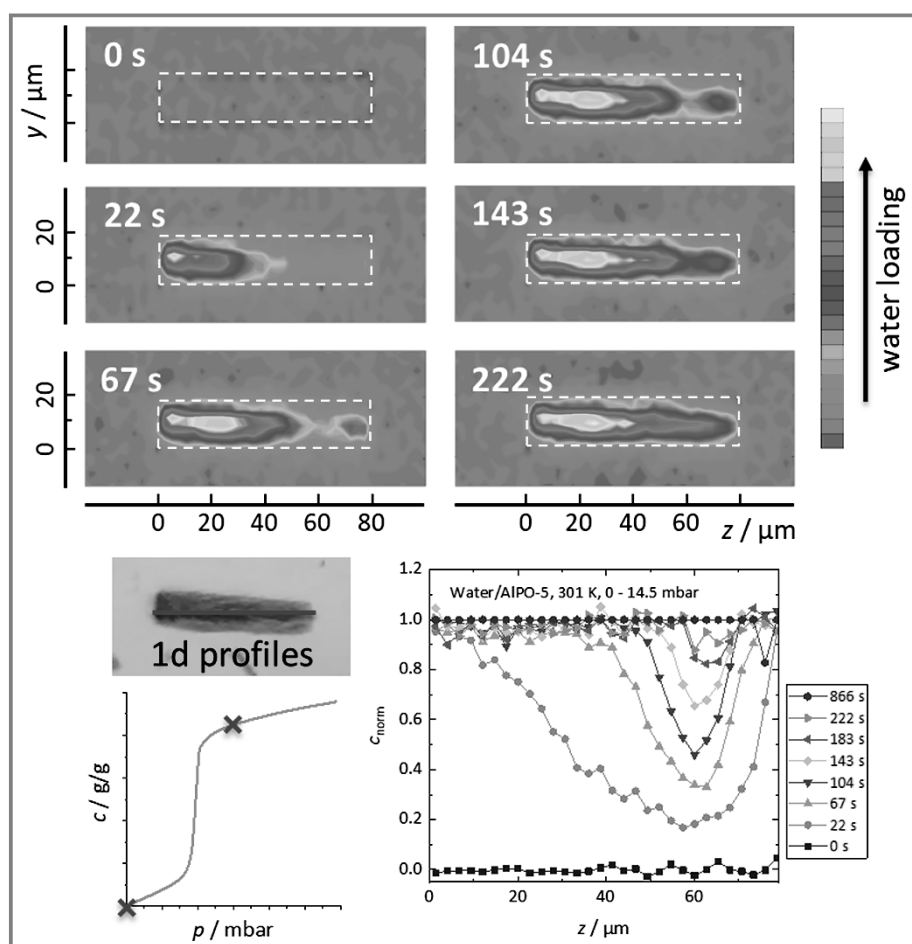


**Figure 7.** IR imaging of water adsorption in a single AlPO-5 crystal (length ca. 80  $\mu\text{m}$ ) for a large loading step at 301 K (top). The approximate dimensions of the crystal are included as dashed box as guide for the eye. The one-dimensional representation of sections normalized to the final profile along the longitudinal axis of the crystal (bottom right) clearly shows that the left half of the crystal is already completely filled after 1 min, while this is the case in the right half of the crystal only after about 5 min.

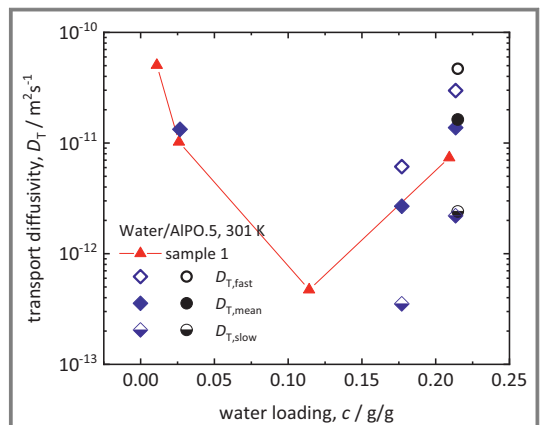


**Figure 8.** Comparison of the diffusion coefficients of water in two different AlPO-5 crystals estimated from the IR imaging measurements with the data from previous integral uptake measurements. Both halves of the crystal were evaluated separately for each measurement, with the ratio  $D_{\text{T},\text{fast}}/D_{\text{T},\text{slow}}$  being in the range of 10–25. The mean values from imaging agree very well with the data from integral uptake.

Interestingly, this factor of 10–25 roughly corresponds to the difference predicted by MD simulations for the diffusion coefficients in AlPO-5 in different framework phase states

[43]. However, since the mass transport in the IRM measurements is most likely dominated by defects, it remains to be clarified if phase changes of the regular lattice can have an equivalent influence on IRM diffusivities. If phase changes are involved it also has to be clarified why the two crystal halves behave differently with regard to phase changes.

#### 4 Conclusions

This contribution presents the first direct observation of water diffusion inside crystals of AlPO-5 by means of PFG NMR and IRM. Combination of these two techniques in a complimentary way enables quantification of the propagation of water on the industrial-relevant time- and length scales, i.e., from milliseconds to seconds and from 1 to 100  $\mu\text{m}$ . The water self-diffusion coefficients inside AlPO-5 crystals probed by PFG NMR revealed a very good agreement with previously reported data from quasi-elastic neutron scattering suggesting absence of structural defects on a scale of  $\sim 1 \mu\text{m}$ . However, further studies by IRM resulted in values of corrected diffusivity approximately one order of magnitude lower at comparable hydration levels and

temperature. This observation is attributed to the existence of defects on the length scale of few tens of micrometers, being important for heat storage systems utilizing AlPO-5 crystals of this size or larger.

## Acknowledgment

We would like to express our heartfelt appreciation to Prof. Dr. Jörg Kärger on the occasion of his 80th birthday. His pioneering contributions to the field of microscopic diffusion measurements have left an indelible mark on our understanding and have inspired generations of researchers. Professor Kärger's unwavering dedication to advancing knowledge and his exceptional mentorship have had a profound impact on the academic journeys of C.C. and M.D. We are grateful for his invaluable guidance, wisdom, and for being a true beacon of excellence in our scientific community.

All authors gratefully acknowledge the financial support of BMBF, project 03SF0552B "Wassermod2". Authors also thank very much Andreas Kuhnt, FAHRENHEIT GmbH, Dr. Georgios N. Karanikolos, Department of Chemical Engineering, Khalifa University, and Dr. Charitomeni M. Veziri, Institute of Nanoscience & Nanotechnology, Demokritos National Research Center, for sample synthesis and Dr. David Poppitz, Institute of Chemical Technology, Leipzig University, for SEM characterization of materials. NMR diffusion experiments have been performed in the Felix-Bloch Institute for Solid State Physics, Division of Applied Magnetic Resonance, Leipzig University. Scientific discussions with Prof. Dr. Frank Stallmach are gratefully appreciated. Open access funding enabled and organized by Projekt DEAL.

## Symbols used

$A$	[a.u.]	IR absorbance
$c$	[g g <sup>-1</sup> ]	concentration of guest molecules inside the porous material
$D_T$	[m <sup>2</sup> s <sup>-1</sup> ]	transport (Fickian) diffusivity; indices 'fast' and 'slow' refer to local diffusivities inside AlPO-5 crystals estimated from IRM experiments
$D_0$	[m <sup>2</sup> s <sup>-1</sup> ]	corrected (intrinsic) diffusivity; identical to Maxwell-Stefan
$D_{\text{inter}}$	[m <sup>2</sup> s <sup>-1</sup> ]	diffusivity for single components intercrystalline self-diffusivity, self-diffusivity in the crystal bed/voids between the crystals
$D_{\text{intra}}$	[m <sup>2</sup> s <sup>-1</sup> ]	intracrystalline self-diffusivity, self-diffusivity inside the pores of crystals
$E_A$	[kJ mol <sup>-1</sup> ]	activation energy for diffusion
$g$	[T m <sup>-1</sup> ]	applied field gradient in NMR
$l$	[m]	crystal lengths
$p$	[Pa]	pressure
$p_{\text{intra}}$	[−]	fraction ( $0 \leq p_{\text{intra}} \leq 1$ ) of molecules in the intracrystalline pore space
$T$	[K]	temperature
$t$	[s]	observation time

## Greek letters

$\Delta$	[ms]	separation between two gradient pulses in NMR
$\delta$	[ms]	duration of the gradient pulses in NMR
$\Gamma$	[−]	thermodynamic factor
$\gamma$	[C kg <sup>-1</sup> ]	gyromagnetic ratio of nuclei
$\tau$	[ms]	separation between first two 90° radio-frequency pulses in NMR
$\Psi$	[a.u.]	NMR signal normalized to its maximum value

## Abbreviations

AlPO-5	aluminum phosphate 5, zeolite with AFI-type structure
IRM	infrared microscopy, infrared microimaging
PFG NMR	pulsed field gradient nuclear magnetic resonance
SEM-EDX	scanning electron microscopy with energy dispersive X-ray spectroscopy

## References

- [1] Y. Zhang, R. Wang, *Energy Storage Mater.* **2020**, *27*, 352–369. DOI: <https://doi.org/10.1016/j.ensm.2020.02.024>
- [2] L. F. Cabeza, A. Solé, C. Barreneche, *Renewable Energy* **2017**, *110*, 3–39. DOI: <https://doi.org/10.1016/j.renene.2016.09.059>
- [3] A. A. ElBahloul, E.-S. B. Zeidan, I. I. El-Sharkawy, A. M. Hamed, A. Radwan, *J. Energy Storage* **2022**, *45*, 103683. DOI: <https://doi.org/10.1016/j.est.2021.103683>
- [4] S. K. Henninger, F. P. Schmidt, H.-M. Henning, *Adsorption* **2011**, *17* (5), 833–843. DOI: <https://doi.org/10.1007/s10450-011-9342-6>
- [5] S. K. Henninger, F. P. Schmidt, T. Nunez, H.-M. Henning, *Adsorption* **2005**, *11* (S1), 361–366. DOI: <https://doi.org/10.1007/s10450-005-5951-2>
- [6] J. Jänen, D. Ackermann, H. Stach, W. Brösicke, *Sol. Energy* **2004**, *76* (1–3), 339–344. DOI: <https://doi.org/10.1016/j.solener.2003.07.036>
- [7] U. Wittstadt, G. Füldner, E. Laurenz, A. Warlo, A. Große, R. Herrmann, L. Schnabel, W. Mittelbach, *Renewable Energy* **2017**, *110*, 154–161. DOI: <https://doi.org/10.1016/j.renene.2016.08.061>
- [8] F. Stallmach, T. Splith, C. Chmelik, G. Füldner, S. K. Henninger, P. T. Kolokathis, E. Pantatosaki, G. K. Papadopoulos, *Chem. Ing. Tech.* **2016**, *88* (3), 372–378. DOI: <https://doi.org/10.1002/cite.201500140>

- [9] D. Fröhlich, E. Pantatosaki, P. D. Kolokathis, K. Markey, H. Reinsch, M. Baumgartner, M. A. van der Veen, D. E. de Vos, N. Stock, G. K. Papadopoulos, S. K. Henninger, C. Janiak, *J. Mater. Chem. A* **2016**, *4* (30), 11859–11869. DOI: <https://doi.org/10.1039/C6TA01757F>
- [10] P. D. Kolokathis, E. Pantatosaki, G. K. Papadopoulos, *J. Phys. Chem. C* **2015**, *119* (34), 20074–20084. DOI: <https://doi.org/10.1021/acs.jpcc.5b04284>
- [11] T. Splitth, E. Pantatosaki, P. D. Kolokathis, D. Fröhlich, K. Zhang, G. Füldner, C. Chmelik, J. Jiang, S. K. Henninger, F. Stallmach, G. K. Papadopoulos, *J. Phys. Chem. C* **2017**, *121* (33), 18065–18074. DOI: <https://doi.org/10.1021/acs.jpcc.7b06240>
- [12] U. Wittstadt, G. Füldner, O. Andersen, R. Herrmann, F. Schmidt, *Energies* **2015**, *8* (8), 8431–8446. DOI: <https://doi.org/10.3390/en8088431>
- [13] C. Lehmann, S. Beckert, R. Gläser, O. Kolditz, T. Nagel, *Appl. Energy* **2017**, *185*, 1965–1970. DOI: <https://doi.org/10.1016/j.apenergy.2015.10.126>
- [14] Y. I. Aristov, *Appl. Therm. Eng.* **2013**, *50* (2), 1610–1618. DOI: <https://doi.org/10.1016/j.applthermaleng.2011.09.003>
- [15] Y. Aristov, *Appl. Therm. Eng.* **2014**, *72* (2), 166–175. DOI: <https://doi.org/10.1016/j.applthermaleng.2014.04.077>
- [16] J. Jänenchen, H. Stach, U. Hellwig, in *Zeolites and related materials: Trends, targets and challenges, Proceedings of the 4th International FEZA Conference*, Vol. 174, Studies in Surface Science and Catalysis, Elsevier, Amsterdam **2008**.
- [17] A. Ristić, N. Z. Logar, S. K. Henninger, V. Kaučič, *Adv. Funct. Mater.* **2012**, *22* (9), 1952–1957. DOI: <https://doi.org/10.1002/adfm.201102734>
- [18] F. Jeremias, A. Khutia, S. K. Henninger, C. Janiak, *J. Mater. Chem.* **2012**, *22* (20), 10148–10151. DOI: <https://doi.org/10.1039/C2JM15615F>
- [19] S. K. Henninger, S.-J. Ernst, L. Gordeeva, P. Bendix, D. Fröhlich, A. D. Grekova, L. Bonaccorsi, Y. Aristov, J. Jaenchen, *Renewable Energy* **2017**, *110*, 59–68. DOI: <https://doi.org/10.1016/j.renene.2016.08.041>
- [20] S. Beckert, F. Stallmach, H. Toufar, D. Freude, J. Kärger, J. Haase, *J. Phys. Chem. C* **2013**, *117* (47), 24866–24872. DOI: <https://doi.org/10.1021/jp408604y>
- [21] A. Lauerer, R. Kurzhals, H. Toufar, D. Freude, J. Kärger, *J. Magn. Reson.* **2018**, *289*, 1–11. DOI: <https://doi.org/10.1016/j.jmr.2018.01.011>
- [22] C. Chmelik, H. Voß, H. Bux, J. Caro, *Chem. Ing. Tech.* **2011**, *83* (1–2), 104–112. DOI: <https://doi.org/10.1002/cite.201000179>
- [23] T. Chokbunpiam, S. Fritzsche, C. Chmelik, J. Caro, W. Janke, S. Hannongbua, *Chem. Phys. Lett.* **2016**, *648*, 178–181. DOI: <https://doi.org/10.1016/j.cplett.2016.01.060>
- [24] C. M. Veziri, M. Palomino, G. N. Karanikolos, A. Corma, N. K. Kanellopoulos, M. Tsapatsis, *Chem. Mater.* **2010**, *22* (4), 1492–1502. DOI: <https://doi.org/10.1021/cm902569g>
- [25] M. Russina, G. Günther, V. Grzimek, M. C. Schlegel, C. M. Veziri, G. N. Karanikolos, T. Yamada, F. Mezei, *J. Phys. Chem. Lett.* **2019**, *10* (20), 6339–6344. DOI: <https://doi.org/10.1021/acs.jpclett.9b02303>
- [26] D. Kong, Y. Liu, J. Zhang, H. Li, X. Wang, G. Liu, B. Li, Z. Xu, *New J. Chem.* **2014**, *38* (7), 3078–3083. DOI: <https://doi.org/10.1039/c4nj00034j>
- [27] F. Stallmach, J. Kärger, *Adsorption* **1999**, *5* (2), 117–133. DOI: <https://doi.org/10.1023/A:1008949607093>
- [28] J. Kärger, T. Binder, C. Chmelik, F. Hibbe, H. Krautscheid, R. Krishna, J. Weitkamp, *Nat. Mater.* **2014**, *13* (4), 333–343. DOI: <https://doi.org/10.1038/nmat3917>
- [29] J. Kärger, D. M. Ruthven, D. N. Theodorou, *Diffusion in Nanoporous Materials*, Wiley-VCH, Weinheim **2012**.
- [30] *Verified Syntheses of Zeolithic Materials* (Eds: H. Robson, K. P. Lilierud), Elsevier, Amsterdam **2001**.
- [31] V. Kukla, J. Kornatowski, D. Demuth, I. Girius, H. Pfeifer, L. V. Rees, S. Schunk, K. K. Unger, J. Kärger, *Science* **1996**, *272* (5262), 702–704. DOI: <https://doi.org/10.1126/science.272.5262.702>
- [32] S. S. Nirvarthi, A. V. McCormick, H. Davis, *Chem. Phys. Lett.* **1994**, *229* (3), 297–301. DOI: [https://doi.org/10.1016/0009-2614\(94\)01059-5](https://doi.org/10.1016/0009-2614(94)01059-5)
- [33] M. Holz, S. R. Heil, A. Sacco, *Phys. Chem. Chem. Phys.* **2000**, *2* (20), 4740–4742. DOI: <https://doi.org/10.1039/B005319H>
- [34] F. G. Alabarse, J. Haines, O. Cambon, C. Levelut, D. Bourgogne, A. Haidoux, D. Granier, B. Coasne, *Phys. Rev. Lett.* **2012**, *109* (3), 35701. DOI: <https://doi.org/10.1103/PhysRevLett.109.035701>
- [35] A. Feldhoff, J. Caro, H. Jobic, J. Ollivier, C. B. Krause, P. Galvásas, J. Kärger, *ChemPhysChem* **2009**, *10* (14), 2429–2433. DOI: <https://doi.org/10.1002/cphc.200900279>
- [36] H. Jobic, M. Bee, J. Kärger, C. Balzer, A. Julbe, *Adsorption* **1995**, *1* (3), 197–201. DOI: <https://doi.org/10.1007/BF00704223>
- [37] H. Jobic, M. Bée, J. Caro, M. Bülow, J. Kärger, *J. Chem. Soc., Faraday Trans. 1* **1989**, *85* (12), 4201. DOI: <https://doi.org/10.1039/f19898504201>
- [38] H. Jobic, H. Ernst, W. Heink, J. Kärger, A. Tuel, M. Bée, *Microporous Mesoporous Mater.* **1998**, *26* (1–3), 67–75. DOI: [https://doi.org/10.1016/S1387-1811\(98\)00216-9](https://doi.org/10.1016/S1387-1811(98)00216-9)
- [39] H. Jobic, W. Schmidt, C. B. Krause, J. Kärger, *Microporous Mesoporous Mater.* **2006**, *90* (1–3), 299–306. DOI: <https://doi.org/10.1016/j.micromeso.2005.10.020>
- [40] J. Kärger, H. Jobic, *Colloids Surf.* **1991**, *58* (1–2), 203–205. DOI: [https://doi.org/10.1016/0166-6622\(91\)80208-6](https://doi.org/10.1016/0166-6622(91)80208-6)
- [41] H. Paoli, A. Méthivier, H. Jobic, C. Krause, H. Pfeifer, F. Stallmach, J. Kärger, *Microporous Mesoporous Mater.* **2002**, *55* (2), 147–158. DOI: [https://doi.org/10.1016/S1387-1811\(02\)00399-2](https://doi.org/10.1016/S1387-1811(02)00399-2)
- [42] R. Krishna, *Chem. Soc. Rev.* **2012**, *41* (8), 3099–3118. DOI: <https://doi.org/10.1039/C2CS15284C>
- [43] P. D. Kolokathis, T. Nonnen, G. Füldner, G. K. Papadopoulos, *Microporous Mesoporous Mater.* **2022**, *329*, 111501. DOI: <https://doi.org/10.1016/j.micromeso.2021.111501>
- [44] C. Chmelik, H. Bux, J. Caro, L. Heinke, F. Hibbe, T. Titze, J. Kärger, *Phys. Rev. Lett.* **2010**, *104* (8), 85902. DOI: <https://doi.org/10.1103/PhysRevLett.104.085902>
- [45] L. Karwacki, H. E. van der Bij, J. Kornatowski, P. Cubillas, M. R. Drury, D. A. M. de Winter, M. W. Anderson, B. M. Weckhuysen, *Angew. Chem., Int. Ed.* **2010**, *49* (38), 6790–6794. DOI: <https://doi.org/10.1002/anie.201003273>
- [46] G. J. Klap, M. Wübbnenhorst, J. C. Jansen, H. van Koningsveld, H. van Bekkum, J. van Turnhout, *Chem. Mater.* **1999**, *11* (12), 3497–3503. DOI: <https://doi.org/10.1021/cm9910431>
- [47] E. Lehmann, C. Chmelik, H. Scheidt, S. Vasenkov, B. Staudte, J. Kärger, F. Kremer, G. Zadrožna, J. Kornatowski, *J. Am. Chem. Soc.* **2002**, *124* (29), 8690–8692. DOI: <https://doi.org/10.1021/ja026400z>
- [48] E. Lehmann, S. Vasenkov, J. Kärger, G. Zadrožna, J. Kornatowski, Ö. Weiss, F. Schüth, *J. Phys. Chem. B* **2003**, *107* (20), 4685–4687. DOI: <https://doi.org/10.1021/jp034616x>
- [49] R. Herrmann, W. Schwieger, J. Bauer, *Patent EP2403977B1*, 2010.